 doi:10.20944/preprints202009.0507.v1

Article

Influence of Thermoelastic Phenomena on the Energy Conservation in Non-contacting Face Seals

Slawomir Blasiak *

Kielce University of Technology, Faculty of Mechatronics and Mechanical Engineering, Department of Manufacturing Engineering and Metrology, Aleja Tysiaclecia Panstwa Polskiego 7, 25-314 Kielce, Poland
* Correspondence: sblasiak@tu.kielce.pl; Tel.: +48-41-34-24-756

Abstract: The purpose of this study was to develop a mathematical model for non-contacting face seals to analyze how their performance is affected by thermoelastic phenomena. The model was used to solve thermal conductivity and thermoelasticity problems. The primary goal was to calculate the values of thermal deformations of the sealing rings in a non-contacting face seal with a flexibly mounted rotor (FMR) for a turbomachine. The model assumes conversion of mechanical energy into heat in the fluid film. The heat flux generated in the fluid film is transferred first to the sealing rings and then to the fluid surrounding them. An asymmetric distribution of temperature within the sealing rings leads to the occurrence of thermal stresses and, consequently, a change in the rings geometry. The model is solved analytically. The distributions of temperature fields for the sealing rings in the cross-sections are calculated using the Fourier-Bessel series as a superficial function of two variables (r,z). The thermoelasticity problems described by the Navier equations are solved by applying the Boussinesq harmonic functions and Goodier's thermoelastic displacement potential function. The proposed method involves solving various theoretical and practical problems of thermoelasticity in FMR-type non-contacting face seals. The calculated thermal deformations of the sealing rings are used to determine the most important seal performance parameters such as the leakage rate and power loss.

Keywords: mechanical seal; non-contacting face seal; heat transfer; thermal analysis

1. Introduction

This article provides an analytical solution to an axisymmetric thermoelastic problem for sealing rings in non-contacting face seals. The basic requirement concerning the performance of non-contacting seals is to maintain the height of the radial clearance within the limits determined at the design stage. This is difficult to achieve because of different disturbances affecting the seal performance. The most important are disturbances to the equilibrium of forces acting on the system of rings, which may be caused, for example, by thermal deformations of these elements.

There is plenty of research into the behavior of non-contacting seals. This article reviews only studies focusing on heat transfer and thermal deformations.

Some of the first research papers on the subject provided mathematical descriptions of the heat transfer phenomena in non-contacting seals in the form of one-dimensional models; they analyzed only the distributions of pressure and temperature within the sealing rings and the fluid film (e.g., [1]). Then, more complex thermohydrodynamic and thermoelastohydrodynamic models were proposed. Refs. [2–6], for instance, discuss numerical solutions to advanced two- and three-dimensional mathematical models.

Studies on thermoelastic problems for non-contacting seals include Ref. [7], which provides numerical calculations of thermal deformations of the sealing rings to analyze their effect on the seal performance. Ref. [8] describes two types of macroscopic thermoelastic deformations: those taking place under quasi-steady state conditions and those typical of unsteady state conditions. The latter,

Preprints (www.preprints.org) | NOT PEER-REVIEWED | Posted: 22 September 2020 doi:10.20944/preprints202009.0507.v1

referred to as thermoelastic instability, are sudden uncontrolled deformations of the surface of the sealing rings. The experiments confirmed the occurrence of both types of thermal deformation.

The geometry of the clearance between the sealing rings changes when the elements are deformed; this disturbs the equilibrium of forces and causes changes in the leakage rate and power loss.

This article proposes a two-dimensional model to describe the heat transfer and thermal deformations in non-contacting face seals. The equations with partial derivatives are solved using the technique of separation of variables. For both rings, the equation of energy and equations of conductivity are written in a cylindrical coordinate system, and the analytical solutions are based on the Bessel functions of the first and second kind. The thermoelasticity problems described by the Navier equations are solved using the Boussinesq harmonic functions as well as Goodier's thermoelastic displacement potential function.

Because of their specific design and varied operating conditions, non-contacting seals are vital elements of sealing systems in a variety of machines. The proposed solution of the complex mathematical model is used to analyze the effect of thermal deformations on the basic seal performance parameters, i.e., leakage rate and power loss.

2. Mathematical model

Error! Reference source not found. shows a schematic diagram of an FMR-type non-contacting face seal. The seal consists of two rings: a rotor (2), flexibly mounted to the shaft (6) of the turbomachine, and a stator (1), fixed to the housing.

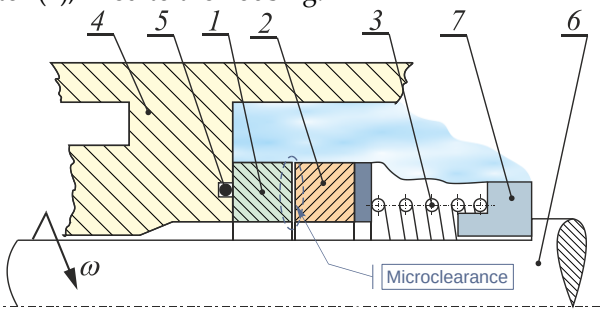

Figure 1. Non-contacting face seal: 1 – stator, 2 – rotor, 3 – spring, 4 – housing, 5 – O-ring, 6 – shaft 7 – steady pin.

The mathematical model describing the physical phenomena occurring in the sealing rings–fluid film system of a non-contacting face seal was developed using some simplifications, like in [9–12]. The formulated model was then solved analytically.

2.1. Function of the radial clearance height

A key parameter of non-contacting face seals is the nominal height of the radial clearance h_o, which is dependent on the equilibrium of forces acting on the sealing rings. The geometry of the fluid film separating the rings can be written as a difference between the functions of the surface topographies of the rotor and stator. The general form of the function is:

$$h = h(r) = h_o + h^r(r) - h^s(r) + h(r)^r_{def} - h(r)^s_{def} \quad (1)$$

Although there are many theoretical studies on the subject providing models of heat transfer in the rotor-stator system, they do not take into consideration changes in the geometry of the radial clearance resulting from the thermal deformations of the rings. In Eq. (1), the relationships $h(r)^r_{def}$ and $h(r)^s_{def}$ represent deformations of the seal faces caused by nonuniform distributions of temperature within the sealing rings.

2.2. Reynolds equation

Preprints (www.preprints.org) | NOT PEER-REVIEWED | Posted: 22 September 2020 doi:10.20944/preprints202009.0507.v1

The distribution of the fluid pressure in the clearance was determined by solving the following one-dimensional Reynolds equation:

$$\frac{d}{dr}\left(\frac{\rho h^3}{\mu}\frac{dp}{dr}\right)=0, \tag{2}$$

where: p – distribution of fluid pressure in the clearance, ρ – fluid density, μ – fluid dynamic viscosity, h – clearance height along the radial coordinate r.

Solving Eq. (2) requires specifying the boundary conditions for the inner and outer radii of the radial clearance. Variables p, ρ and μ are functions dependent on the changes in the fluid temperature in the clearance, whereas the h function is the height of the radial clearance described by Eq. (1).

2.3. Equation of energy

According to the classical hypothesis on thin viscous fluid films, with the fluid being incompressible and in the steady state, the equation of energy for the process fluid takes the following form [2]:

$$\rho c_v\left\{v_r\frac{\partial T^f}{\partial r}+\frac{v_\theta}{r}\frac{\partial T^f}{\partial \theta}+v_z\frac{\partial T^f}{\partial z}\right\}=\mu\left\{\left(\frac{\partial v_r}{\partial z}\right)^2+\left(\frac{\partial v_\theta}{\partial z}\right)^2\right\}+\lambda\frac{\partial^2 T^f}{\partial z^2} \tag{3}$$

After simplifications made for the model of fluid flow in a given type of seal, the equation of energy takes the form [10,13]:

$$\mu\left(\frac{\partial v_\phi}{\partial z}\right)^2+\lambda^f\frac{\partial^2 T^f}{\partial z^2}=0. \tag{4}$$

Once the equation of energy (4) is solved, it is possible to determine the distribution of temperature within the fluid film. The face seal model requires making a simplification concerning the distribution of fluid velocity in the fluid film v_ϕ and an assumption that the velocity changes linearly according to the following relationship [9]:

$$\frac{\partial v_\phi}{\partial z}=\frac{\omega r}{h}. \tag{5}$$

Eq. (5) describes changes in the fluid velocity along the radial clearance height.

2.4. Fluid dynamic viscosity

The fluid dynamic viscosity is largely dependent on the distribution of temperature within the fluid separating the rings; this relationship is provided in [9]. For water, the relationship between fluid viscosity and temperature can be expressed by:

$$\mu=\mu_o\exp\left(-b\left(T_m-T_o\right)\right), \tag{6}$$

The average fluid temperature is defined as:

$$T_m=\frac{1}{h(r)}\int_0^{h(r)}T^f dz. \tag{7}$$

Eq. (6) describes the distribution of fluid dynamic viscosity $\mu(r)$ in the radial direction.

2.5. Distribution of temperature

With axisymmetric heat transfer conditions and constant coefficients of conductivity, the distributions of temperature within the sealing rings can be written in the general form of the equation of conductivity for the steady-state model:

Preprints (www.preprints.org) | NOT PEER-REVIEWED | Posted: 22 September 2020 doi:10.20944/preprints202009.0507.v1

$$\frac{1}{r}\frac{\partial\theta}{\partial r}+\frac{\partial^2\theta}{\partial r^2}+\frac{\partial^2\theta}{\partial z^2}=0\,. \tag{8}$$

Suppose that the difference in temperature θ has no effect on the material coefficients. These can thus be treated as constant. Superscript notation is used, e.g., θ^s and θ^r, for the stator and rotor, respectively.

2.6. Thermoelasticity

The term thermoelasticity refers to a wide range of phenomena. Thermoelasticity represents a generalization of the classical theory of elasticity and the theory of thermal conductivity. In this section, the basic equations describing the thermoelasticity of a homogeneous isotropic body are formulated.

The changes in temperature of the continua, i.e., the ring materials, attributable to the uneven heating of the ring faces, lead to the occurrence of stresses σ_{ij} and strains ε_{ij}; the former can be expressed in the general form using Hooke's law [14]:

$$\sigma_{ij}=2\vartheta\varepsilon_{ij}+\left(\lambda e-\beta\theta\right)\delta_{ij}\quad\left(i,j=1,2,3\right), \tag{9}$$

where the Kronecker symbol is defined as: $\delta_{ij}=\begin{cases}1 & for\ i=j\\ 0 & for\ i\neq j\end{cases}$.

From the equations of equilibrium in the form:

$$\sigma_{ji,j}+F_i=0\qquad\left(i,j=1,2,3\right), \tag{10}$$

as well as Eq. (9) and the defined strains, we can formulate equations of displacement in the general form:

$$\vartheta\nabla^2u_i+\left(\lambda+\vartheta\right)u_{k,ki}-\beta\theta_{,i}+F_i=0\,, \tag{11}$$

where: $\beta=\dfrac{\tau E}{\left(1-2\nu\right)}$, $G=\vartheta$, with the values of the coefficients E and υ being defined in **Error! Reference source not found.**.

Introducing a cylindrical coordinate system $\left(r,\phi,z\right)$ for the axisymmetric problem, we can write the equations of equilibrium of forces (10) in the r and z directions as [14]:

$$\begin{aligned}&\frac{\partial\sigma_{rr}}{\partial r}+\frac{\partial\sigma_{zr}}{\partial z}+\frac{\sigma_{rr}-\sigma_{\phi\phi}}{r}+F_r=0\\&\frac{\partial\sigma_{rz}}{\partial r}+\frac{\partial\sigma_{zz}}{\partial z}+\frac{\sigma_{rz}}{r}+F_z=0\end{aligned} \tag{12}$$

Substituting relationships (9) and the strain components into Eqs. (12) yields a solution to the Navier equations for axisymmetric problems of thermoelasticity, which, when external forces are omitted, can be expressed by means of the thermoelastic displacement potential function Φ and the Boussinesq harmonic functions φ and ψ. The functions must satisfy the following equations:

$$\nabla^2\Phi=K\theta \tag{13}$$

$$\nabla^2\varphi=0,\nabla^2\psi=0\,, \tag{14}$$

with the coefficient K being: $K=\dfrac{1+\upsilon}{1-\upsilon}\tau$

The Michell function M, which is dependent on the Boussinesq harmonic functions:

$$M=-\int\left(\varphi+z\psi\right)dz \tag{15}$$

can be used to write the displacements in the cylindrical coordinate system as [14]:

Preprints (www.preprints.org) | NOT PEER-REVIEWED | Posted: 22 September 2020 doi:10.20944/preprints202009.0507.v1

$$u_r = \frac{\partial \Phi}{\partial r} - \frac{\partial^2 M}{\partial r \partial z} = \frac{\partial \Phi}{\partial r} + \frac{\partial \varphi}{\partial r} + z\frac{\partial \psi}{\partial r}$$
$$u_z = \frac{\partial \Phi}{\partial z} + 2(1-v)\nabla^2 M - \frac{\partial^2 M}{\partial z^2} = \frac{\partial \Phi}{\partial z} + \frac{\partial \varphi}{\partial z} + z\frac{\partial \psi}{\partial z} - (3-4v)\psi \quad . \tag{16}$$

The Michell solution is a biharmonic function satisfying the equation:

$$\nabla^2 \nabla^2 M = -2\nabla^2 \psi = 0 \tag{17}$$

Thus, the stress components are represented by the thermoelastic displacement potential function Φ and the Michell solution M:

$$\sigma_{rr} = 2G\left[\frac{\partial^2 \Phi}{\partial r^2} - K\theta + \frac{\partial}{\partial z}\left(v\nabla^2 M - \frac{\partial^2 M}{\partial r^2}\right)\right]$$
$$\sigma_{\phi\phi} = 2G\left[\frac{1}{r}\frac{\partial \Phi}{\partial r} - K\theta + \frac{\partial}{\partial z}\left(v\nabla^2 M - \frac{1}{r}\frac{\partial M}{\partial r}\right)\right]$$
$$\sigma_{zz} = 2G\left[\frac{\partial^2 \Phi}{\partial z^2} - K\theta + \frac{\partial}{\partial z}\left((2-v)\nabla^2 M - \frac{\partial^2 M}{\partial z^2}\right)\right] \tag{18}$$
$$\sigma_{rz} = 2G\left[\frac{\partial^2 \Phi}{\partial r \partial z} + \frac{\partial}{\partial r}\left((1-v)\nabla^2 M - \frac{\partial^2 M}{\partial z^2}\right)\right]$$

$$\sigma_{zz} = \sigma_{rz} = 0 \tag{19}$$

Like in [14], the fields of stresses and displacements are determined using the boundary conditions for Eq. (19), which are such that the surfaces of the rotor $(z=0)$ and the stator $(z=-L)$ are free from stresses.

3. Boundary conditions

The system of coupled equations describing the distributions of temperature within the sealing rings and the radial clearance separating them is solved by imposing the boundary conditions.

The equations of conductivity and equations of energy are solved using suitable boundary conditions, like in [2,10,15]. The boundary conditions for the system considered are shown in **Error! Reference source not found.**.

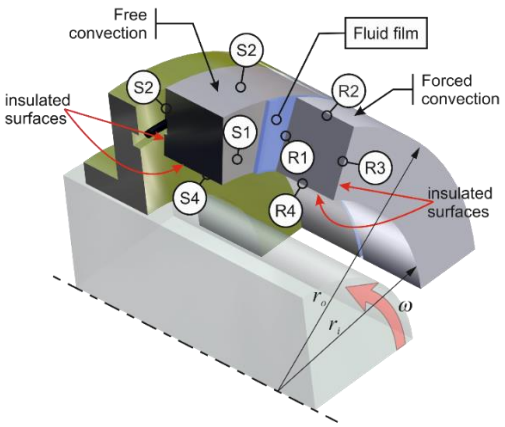

Figure 2. Heat transfer conditions for the FMR-type non-contacting face seal, where: S_1, S_2, S_3, S_4 – surfaces of the stator and R_1, R_2, R_3, R_4 – surfaces of the rotor.

Preprints (www.preprints.org) | NOT PEER-REVIEWED | Posted: 22 September 2020 doi:10.20944/preprints202009.0507.v1

It is assumed that the surfaces S_3 and S_4 of the stator mounted to the housing and the surfaces R_3 and R_4 of the rotating ring are completely separated so there is no transfer of heat to the fluid surrounding the rings. This condition for both the stator and rotor can be written in the general form as:

$$\frac{\partial \theta}{\partial n} = 0 . \tag{20}$$

Another assumption is that the heat transfer across the surfaces S_1 and R_1 (faces) of the stator and rotor, respectively, which are in direct contact with the fluid filling the radial clearance, occurs by conduction. This implies that the value of the heat flux at the surface of the ring is equal to that of the fluid in the clearance:

$$\lambda^s \frac{\partial \theta^s}{\partial z} = \lambda^f \frac{\partial \theta^f}{\partial z} = q^s{}_v(r) \quad \text{with} \quad \theta^s = \theta^f \quad \text{for } S_1 \tag{21}$$

and

$$q^r{}_v(r) = \lambda^f \frac{\partial \theta^f}{\partial z} = -\lambda^r \frac{\partial \theta^r}{\partial z} \quad \text{with} \quad \theta^f = \theta^r \quad \text{for } R_1. \tag{22}$$

It is also assumed that the heat transfer across the outer surfaces of the rings S_2 and R_2 (**Error! Reference source not found.**), being in contact with the process fluid, takes place by convection. For the stator and rotor, the condition can be written in the general form:

$$-\lambda \left.\frac{\partial \theta}{\partial r}\right|_{r=r_o} = \alpha \theta \big|_{r=r_o} . \tag{23}$$

In the analytical calculations, an additional assumption is made that the heat transfer coefficients for the stator the rotor have different values. This is due to the fact the transfer of heat to the process fluid is higher from the rotating ring than from the stationary ring, with the latter occurring by free convection.

It is assumed that the heat transfer coefficient for the stationary ring has a constant value; the value is given in

For the rotor, the heat transfer coefficient is calculated using relationships [10]:

$$\alpha^r = 0.133 \,\mathrm{Re}_D{}^{2/3} \,\mathrm{Pr}^{1/3} \frac{\lambda^f}{D}, \tag{24}$$

where D is the outer diameter of the seal and Re_D is the Reynolds number based on this diameter; the parameters λ^f and Pr are the thermal conductivity and the Prandtl number of the fluid, respectively.

The Reynolds and Prandtl numbers are described as [16]:

$$\mathrm{Re}_D = \frac{\omega D^2 \rho}{\mu} \tag{25}$$

and

$$\mathrm{Pr} = \frac{C_p \mu}{\lambda^f}, \tag{26}$$

The next section describes the analytical solution of the mathematical model of the heat transfer in non-contacting face seals.

Analytical solution of the heat transfer model

The formulated mathematical model is solved analytically using the technique of separation of variables, like in [17,18]. The first step of the problem-solving process consists of determining the distributions of temperature within the sealing rings by defining the general form of the functions satisfying the differential equation (8) for both the stator and the rotor. Subsequently, a general solution is found to satisfy the specific boundary conditions defined by relationships (20)-(23). The equations describing the distributions of temperature are as follows:

Preprints (www.preprints.org) | NOT PEER-REVIEWED | Posted: 22 September 2020 doi:10.20944/preprints202009.0507.v1

for the stator:

$$T^s = T_0 + \sum_{n=1}^{\infty} B_n^s \cosh\left(s_n^s z^s\right)\left(J_0\left(s_n^s r\right) - \frac{J_1\left(s_n^s r_i\right)}{Y_1\left(s_n^s r_i\right)} Y_0\left(s_n^s r\right)\right), \tag{27}$$

for the fluid film separating the rings:

$$\begin{aligned} T^f = T_0 + \frac{1}{2}\cdot\frac{\mu}{\lambda^f}\cdot\frac{\omega^2\cdot r^2}{h^2}\cdot\left(h^2 - \left(z^f\right)^2\right) + \\ + \sum_{n=1}^{\infty} B_n^r \cosh\left(s_n^r z^r\right)\left(J_0\left(s_n^r r\right) - \frac{J_1\left(s_n^r r_i\right)}{Y_1\left(s_n^r r_i\right)} Y_0\left(s_n^r r\right)\right), \end{aligned} \tag{28}$$

and for the rotor:

$$T^r = T_0 + \sum_{n=1}^{\infty} B_n^r \cosh\left(s_n^r z^r\right)\left(J_0\left(s_n^r r\right) - \frac{J_1\left(s_n^r r_i\right)}{Y_1\left(s_n^r r_i\right)} Y_0\left(s_n^r r\right)\right). \tag{29}$$

The above relationships describing the distributions of temperature within the stator-rotor system and the fluid film will be used to determine the stress fields.

Analytical solution of the thermoelasticity model

The model describing thermoelastic phenomena is relatively complex and its analytical solution requires performing complex calculations. A general method of model solution will be used for both rings. The first stage involves determining the thermoelastic displacement potential function using Eq. (27) or (29), with the superscripts for the stator and rotor being omitted:

$$\theta(r,z) = \sum_{n=1}^{\infty} B_n \cosh\left(s_n z\right)\left(J_0\left(s_n r\right) - \frac{J_1\left(s_n r_i\right)}{Y_1\left(s_n r_i\right)} Y_0\left(s_n r\right)\right). \tag{30}$$

The thermoelastic displacement potential function is written as:

$$\Phi = \frac{K}{2}\sum_{n=1}^{\infty}\frac{B_n}{s_n}(z-L)\sinh\left(s_n z\right)\left(J_0\left(s_n r\right) - \frac{J_1\left(s_n r_i\right)}{Y_1\left(s_n r_i\right)} Y_0\left(s_n r\right)\right). \tag{31}$$

As assumed, the above equation needs to satisfy relationship (13).

The second step requires finding the Michell function. It is predicted to have the following form:

$$M = \frac{K}{2}\sum_{n=1}^{\infty}\frac{B_n}{s_n^3}\left(J_0\left(s_n r\right) - \frac{J_1\left(s_n r_i\right)}{Y_1\left(s_n r_i\right)} Y_0\left(s_n r\right)\right)\begin{pmatrix}(1-2\nu)\sinh\left(s_n z\right)+\\ +(z-L)s_n\cosh\left(s_n z\right)\end{pmatrix}. \tag{32}$$

Substituting these relationships into Eqs. (18) yields the components of the stress tensor:

$$\sigma_{rr} = 4KG\sum_{n=1}^{\infty}\left(\frac{B_n\cosh\left(s_n z\right)\begin{pmatrix}-Y_1\left(s_n r_i\right)J_1\left(s_n r\right)+Y_1\left(s_n r_i\right)J_1\left(s_n r\right)\nu\\ +J_1\left(s_n r_i\right)Y_1\left(s_n r\right)-J_1\left(s_n r_i\right)Y_1\left(s_n r\right)\nu\end{pmatrix}}{Y_1\left(s_n r_i\right)s_n r}\right) \tag{33}$$

$$\sigma_{\phi\phi} = 4GK\sum_{n=1}^{\infty}\left(\frac{B_n\cosh\left(s_n z\right)}{Y_1\left(s_n r_i\right)s_n r}\begin{pmatrix}-s_n r\,Y_1\left(s_n r_i\right)J_0\left(s_n r\right)+s_n r\,J_1\left(s_n r_i\right)Y_0\left(s_n r\right)+\\ +\nu\, s_n r\,J_0\left(s_n r\right)Y_1\left(s_n r_i\right)+\\ -\nu\, s_n r\,J_1\left(s_n r_i\right)Y_0\left(s_n r\right)+\\ +Y_1\left(s_n r_i\right)J_1\left(s_n r\right)-\nu\,Y_1\left(s_n r_i\right)J_1\left(s_n r\right)+\\ -J_1\left(s_n r_i\right)Y_1\left(s_n r\right)+\nu\,J_1\left(s_n r_i\right)Y_1\left(s_n r\right)\end{pmatrix}\right) \tag{34}$$

The relationships describing displacements are given as:

Preprints (www.preprints.org) | NOT PEER-REVIEWED | Posted: 22 September 2020 doi:10.20944/preprints202009.0507.v1

$$u_r = 2K\sum_{n=1}^{\infty} \frac{B_n\left(-1+\nu\right)\left(-Y_1\left(s_n r_i\right)J_1\left(s_n r\right)+J_1\left(s_n r_i\right)Y_1\left(s_n r\right)\right)\cosh\left(s_n z\right)}{Y_1\left(s_n r_i\right)s_n} \quad (35)$$

$$u_z = 2K\sum_{n=1}^{\infty} \frac{B_n\left(-1+\nu\right)\left(-J_0\left(s_n r\right)Y_1\left(s_n r_i\right)+J_1\left(s_n r_i\right)Y_0\left(s_n r\right)\right)\sinh\left(s_n z\right)}{Y_1\left(s_n r_i\right)s_n} \quad (36)$$

The above relationships were used to graphically represent fields of stresses and displacements occurring in the sealing rings due to uneven distributions of temperature.

Results and discussion

A numerical analysis was conducted to verify the relevant hypotheses and assess the influence of the selected parameters on the behavior of non-contacting face seals. In the reference case, water is used as the fluid. The sealing rings are assumed to be in alignment and their faces create a radial clearance with a constant height h_o. Another assumption is that the process fluid is not in contact with the outer surfaces of the rings, except for the cylindrical surfaces, where the heat transfer to the fluid occurs by convection (**Error! Reference source not found.**).

The geometrical and performance parameters of the seal under consideration are defined in **Error! Reference source not found.**

Table 1. Geometrical and performance parameters.

Geometry		Performance parameters	
Inner radius r_i	0.040 (m)	Angular velocity ω	200-1500 (rad/s)
Outer radius r_o	0.045 (m)	Nominal seal clearance h_o	$1{\cdot}10^{-6}$ (m)
Ring thickness L^s and L^r	0.005 (m)	Fluid temperature T_o	20 (^0C)
Thermal conductivity λ^f	0.65 ($W/m\ K$)	Heat transfer coefficient α^s	18000 ($W/m^2\ K$)

One of the first problems mechanical designers need to deal with is selecting the right seal, i.e., a seal that meets the criteria specified for the sealing fluid to be used in the turbomachine, including its temperature and pressure. They must also predict the dry running condition, which takes place during the machine startup and shutdown. Another important problem design engineers have to consider is the chemical durability of the sealing rings and secondary seals. The materials they select for these elements need to have appropriate physicochemical properties. The most common materials used for mechanical seals are characterized in **Error! Reference source not found.**.

Table 2. Properties of materials used for the sealing rings.

	Young's modulus E (GPa)	**Poisson's coefficient ν**	**Thermal conductivity λ (W m^{-1} K^{-1})**	**Linear thermal expansion coefficient τ (10^{-6} °C)**
SiC (Silicon Carbide)	400	0.17	150	4.3
Resin-impregnated carbon	24	0.12	10	4.9
Alumina (Ceramic)	350	0.23	30	7.5
Tungsten carbide (WC)	630	0.24	85	5.4

The materials used for the sealing rings need to be suitable for the seal operating conditions. In the case of non-contacting face seals, the sealing rings are usually made of dissimilar materials, i.e.,

Preprints (www.preprints.org) | NOT PEER-REVIEWED | Posted: 22 September 2020 doi:10.20944/preprints202009.0507.v1

ones differing in physicochemical properties. This, however, leads to the occurrence of a sequence of undesirable phenomena, starting with uneven heat transfer from the radial clearance to the surrounding fluid, followed by asymmetric thermoelastic deformations of the rings, then a change in the geometry of the radial clearance and, finally, an increase in the leakage rate.

Non-contacting face seals, also called mechanical face seals, are used in many mechanical sealing systems. The correct performance of non-contacting seals is conditioned by the properly selected parameters of the sealing rings. One of the most significant parameters that have a direct effect on the distribution of pressure within the fluid film and the heat flux generated in the clearance is the angular velocity of the rotor.

The key feature of mechanical seals is the ability to operate in 'no lubrication' conditions. In practice, this does not last long, but the materials used for the sealing rings must have sufficient hardness and thermal resistance to withstand an increase in temperature caused by excessive friction forces. Two types of material configurations are used for the sealing rings: 'hard-hard' and 'hard-soft'.

Seals with both rings made of hard materials, e.g., silicon carbide-silicon carbide or tungsten carbide-tungsten carbide, exhibit high resistance to many active chemical compounds, but they are characterized by little resistance to dry running. Seals with a hard-soft ring configuration, on the other hand, e.g., carbon-tungsten carbide, are more resistant to dry running, but have limited chemical resistance to fluids other than water. As the selection of ring materials to match the seal operating conditions is an open problem, a numerical analysis is necessary. This study was conducted for two types of rotor materials, i.e., silicon carbide and tungsten carbide, and three types of stator materials, i.e., silicon carbide, tungsten carbide, and a alumina (ceramic). The numerical analysis was thus performed for six pairs of sealing rings.

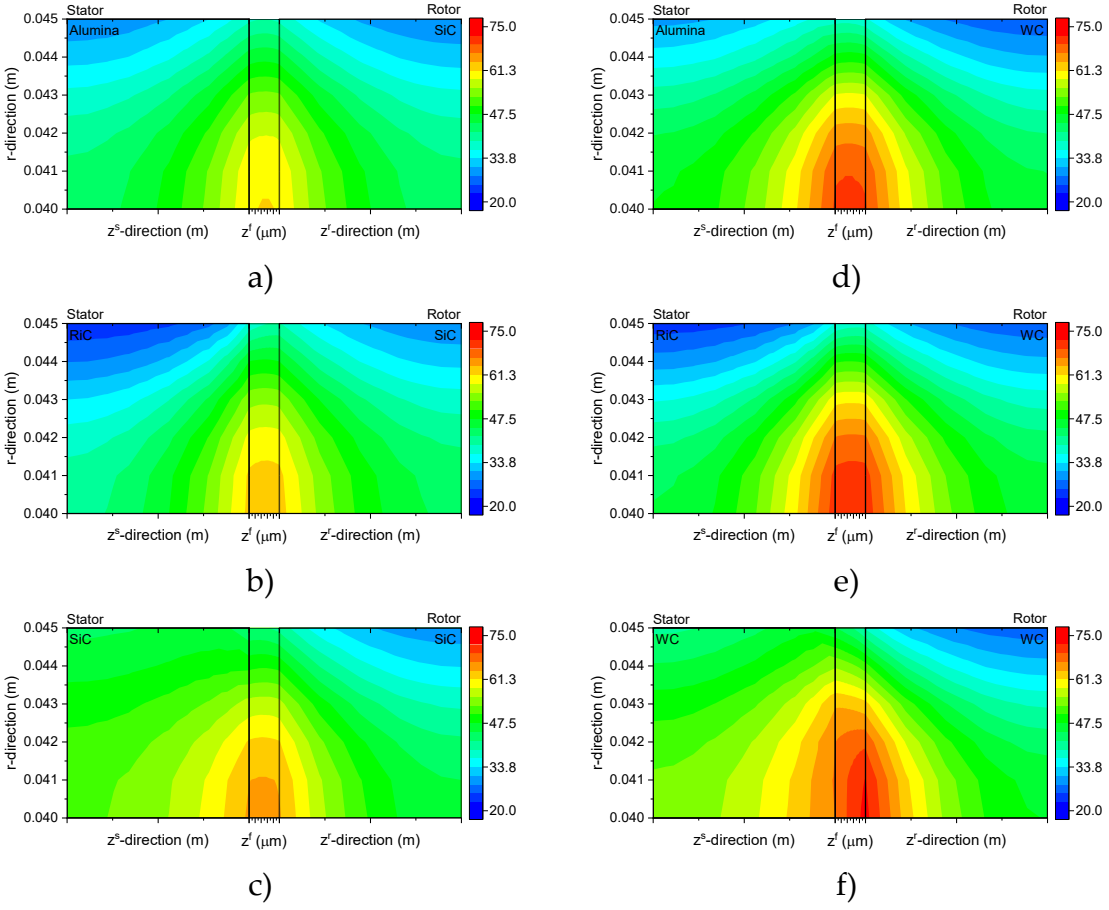

Figure 3. Temperature distributions in the cross-sections of the sealing rings and the fluid film at $\omega = 1500\ \left(\text{rad/s}\right)$

Preprints (www.preprints.org) | NOT PEER-REVIEWED | Posted: 22 September 2020 doi:10.20944/preprints202009.0507.v1

The diagrams in **Error! Reference source not found.** illustrate temperature distributions in the cross-sections of the sealing rings and the fluid film separating them. The results show that, in all the cases considered, the maximum temperature of the fluid film is registered along the inner radius r_i, which is directly related to the heat transfer model. Depending on the material configuration, the temperature there ranges from 61.4? 1.6 ^oC at an angular velocity of 1500 (rad/s). The lowest temperature of the fluid film is reported for the Alumina-SiC pair (**Error! Reference source not found.**a), while the highest for the RiC-WC and WC-WC pairs (**Error! Reference source not found.**e and f). Another observation is a large difference in temperature along the outer radius r_o. It should be noted that the analyzed model assumes forced convection for the rotor, which implies increased heat transfer to the fluid surrounding this ring. From **Error! Reference source not found.**b and e, it is evident that, for the RiC-SiC and RiC-WC pairs, the temperature along the outer radius is up to 5 ^oC lower for the stator than for the rotor. When the stator and rotor are made of the same material, i.e., for the SiC-SiC and WC-WC pairs (**Error! Reference source not found.**c and f), the situation is opposite; the temperature of the stator along the outer radius is 15 ^oC higher than that of the rotor. It is important that the temperature differences in the ring cross-sections be reduced to a minimum to ensure minimum thermal stresses.

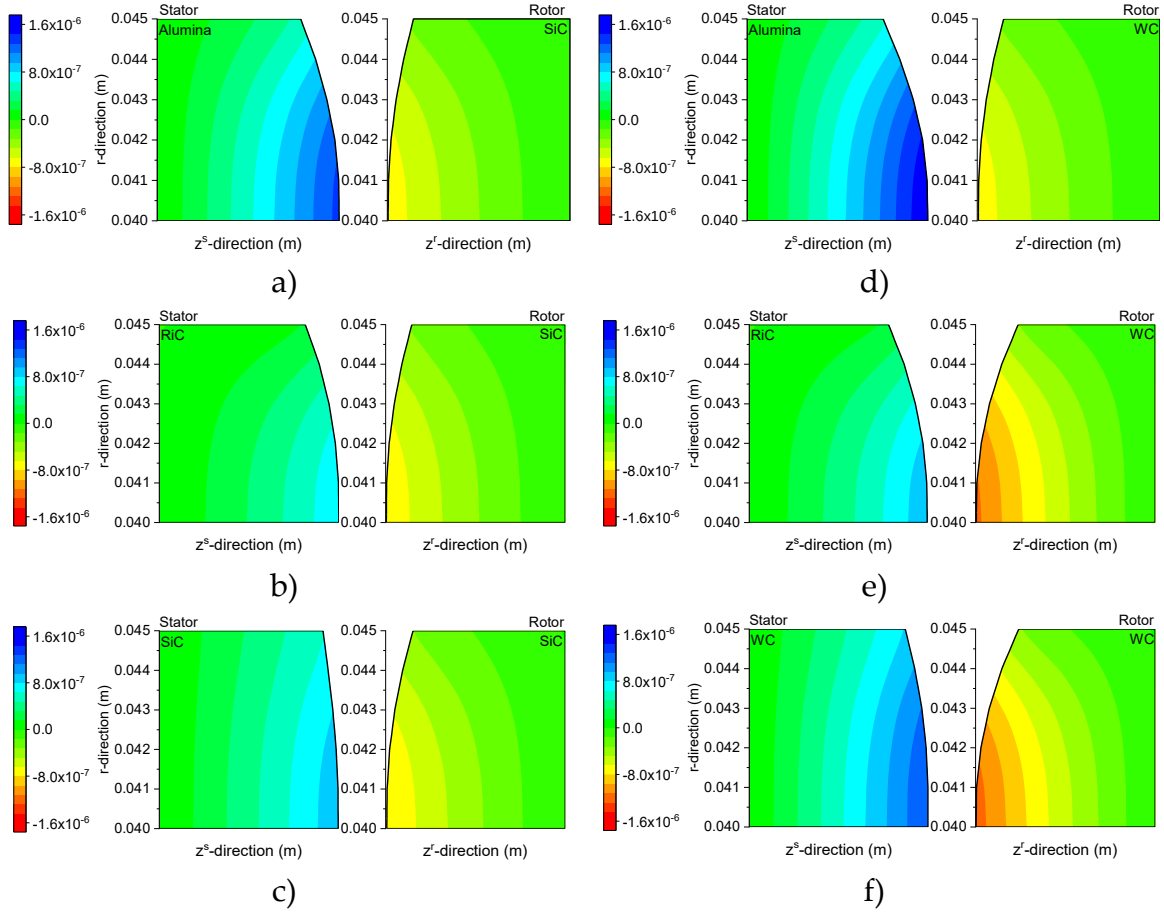

Figure 4. Distributions of axial displacements in the cross-sections of the sealing rings at $\omega = 1500\ (\mathrm{rad/s})$.

Error! Reference source not found. shows the fields of angular displacements in the sealing rings. Since the displacements were very small, of the order of $10^{-6}\,(m)$, the deformations of the rings caused by thermal stresses were magnified 2000-fold. Thanks to that it is possible to observe warps on the sealing rings. The numerical data indicate that the highest displacements of the order of $1.210^{-6}\,(m)$ occur along the inner radii of the rings in a seal where both the stator and the rotor are made of tungsten carbide (**Error! Reference source not found.**f)

Preprints (www.preprints.org) | NOT PEER-REVIEWED | Posted: 22 September 2020 doi:10.20944/preprints202009.0507.v1

A change in the geometry of the sealing rings causes a change in the height of the radial clearance, taken into consideration in relationships (1), and a change in the distribution of pressure, calculated using the Reynolds equation.

Error! Reference source not found. provides a graphical representation of a change in the function of the radial clearance height, taking account of the thermal deformations of the sealing rings resulting from the asymmetric distribution of temperature in these elements. For each case considered, there is an increase in the minimum height of the radial clearance; the highest value of $1.72 \cdot 10^{-6} \left(m \right)$ is reported for the Alumina-WC pair whereas the lowest of $1.43 \cdot 10^{-6} \left(m \right)$ is observed for the SiC-SiC pair. A change in the geometry of the radial clearance has a direct effect on the distribution of pressure in the fluid film (**Error! Reference source not found.**b), which causes an increase in the opening force.

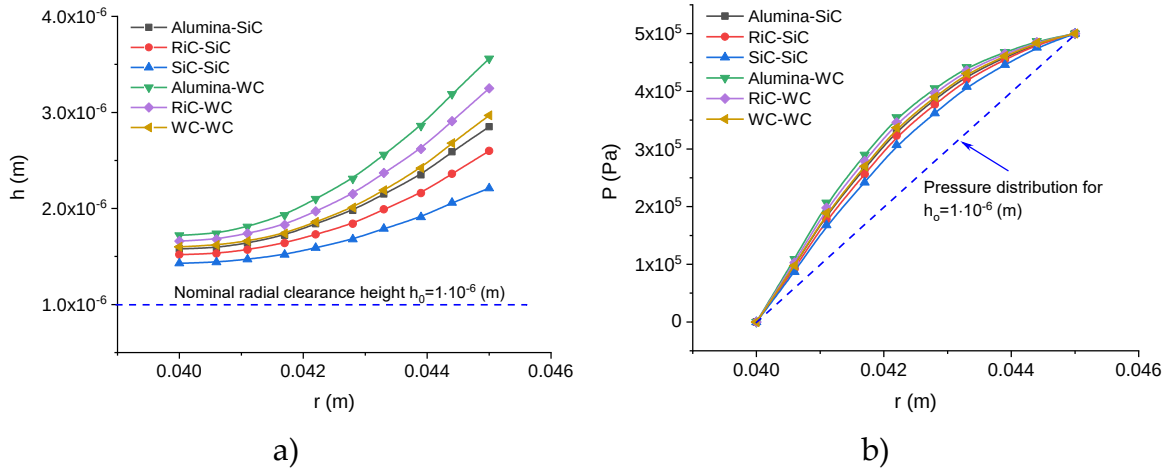

Figure 5. Clearance height and the fluid pressure distribution versus the ring radius at $\omega = 1500 \ \left(\text{rad/s} \right)$

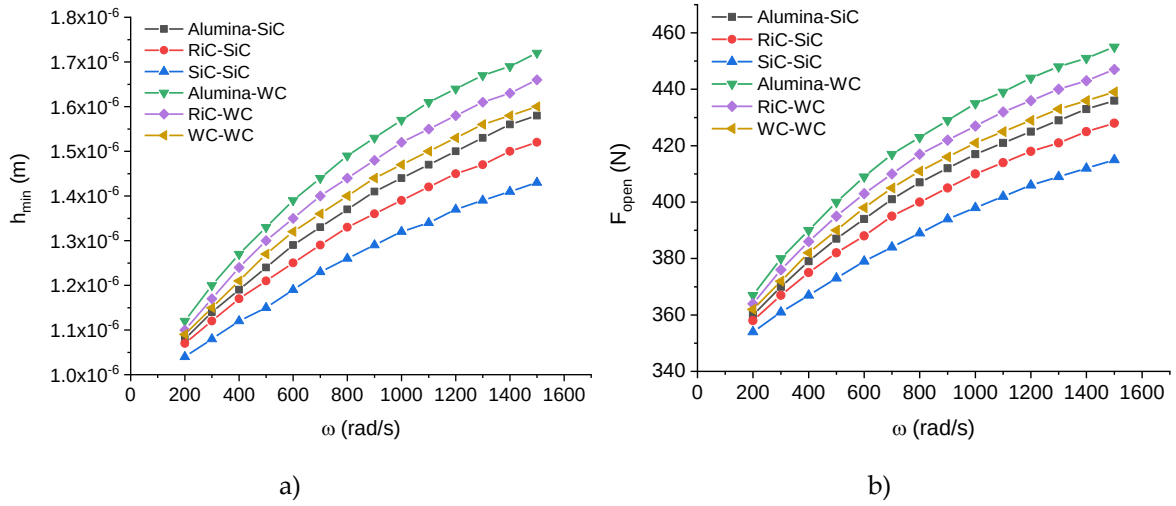

Figure 6. a) Minimum radial clearance height and b) opening force against the angular velocity of the shaft.

Error! Reference source not found. shows changes in the minimum height of the radial clearance and the opening force against the angular velocity of the machine shaft. An increase in this parameter causes an increase in the heat flux generated in the fluid film, according to relationship (4). As a consequence, there is a rise in the temperature of the sealing rings–fluid film system, which is responsible for thermal deformations of the sealing rings, then a change in the geometry of the radial clearance and, finally, an increase in the fluid film pressure. All this leads to a greater radial force

Preprints (www.preprints.org) | NOT PEER-REVIEWED | Posted: 22 September 2020 doi:10.20944/preprints202009.0507.v1

generated in the fluid film and a greater minimum distance between the sealing rings, as shown in Fig. 6.

Power loss results mainly from the viscous shearing of the fluid film between the mating surfaces; it can be calculated from the following relationship [19]:

$$P_{loss} = \int_0^{2\pi} \int_{r_i}^{r_o} \frac{\mu \omega^2 r^2}{h} r dr d\theta \tag{37}$$

The key parameter of the performance of non-contacting face seals is the fluid leakage rate, which is largely attributable to a change in the geometry of the radial clearance and it is described with the following formula:

$$Q_v = \left(r \int_0^{2\pi} -\frac{h^3}{12\mu} \frac{\partial p}{\partial r} d\theta \right) \Bigg|_{r=r_i} \tag{38}$$

As shown in the Fig. 7, the geometry of the clearance changes with changing temperature. **Error! Reference source not found.** shows curves of the volumetric flow rate and power loss against the angular velocity of the shaft.

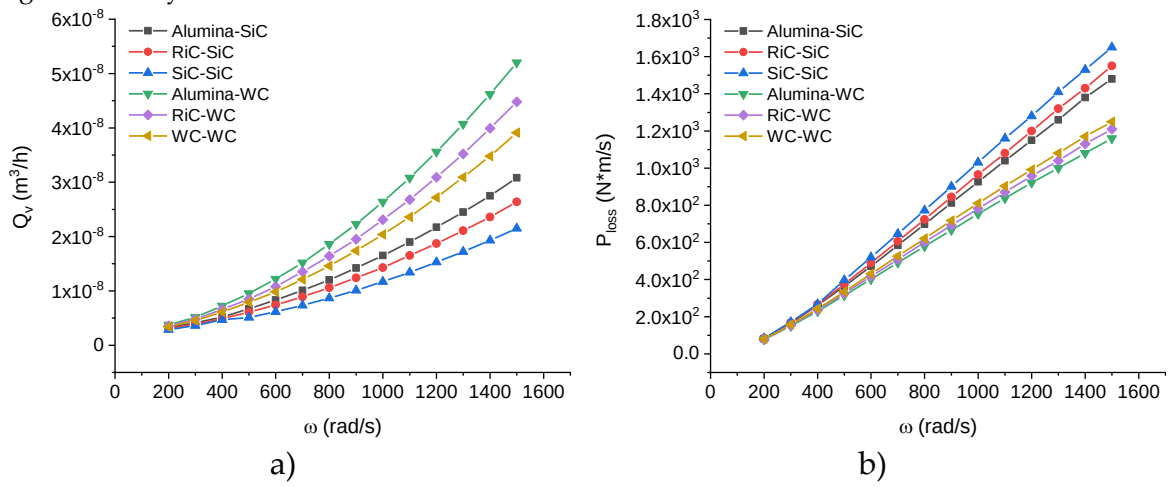

Figure 7. Volumetric flow rate and power loss versus the angular velocity of the shaft.

From the curves in **Error! Reference source not found.**, it is apparent that, when the angular velocity is low, i.e., $\omega = 300\left(rad/s\right)$, the leakage rate and the power loss are very small for all the material pairs considered. An increase in the angular velocity causes an almost linear increase in the power loss in the stator-rotor system and an increase in the leakage rate. At $\omega = 1500\left(rad/s\right)$, the maximum leakage rate is: $Q_v = 2.15 \cdot 10^{-8}\left(m^3/h\right)$ for the SiC–SiC pair and $Q_v = 5.2 \cdot 10^{-8}\left(m^3/h\right)$ for the Alumina-WC pair. At that angular velocity, i.e., $\omega = 1500\left(rad/s\right)$, there may be a double difference in the leakage rate between some pairs of materials.

In the case of power loss, the situation is opposite. An increase in the height of the radial clearance leads to a decrease in the power loss, as illustrated in **Error! Reference source not found.**a and **Error! Reference source not found.**b.

The results suggest that omitting thermal deformations is too great a simplification of the model of non-contacting seals.

It should be noted that the values and character of thermal deformations are in agreement with the numerical results presented, for example, in [7].

Multi-criteria analysis

The multi-criteria analysis is a method used to facilitate the decision-making process when many variants are analyzed to select the best. In this case, the most appropriate pair of materials for the sealing rings is chosen. It is important to note that the criteria used in this analysis were selected and

Preprints (www.preprints.org) | NOT PEER-REVIEWED | Posted: 22 September 2020 doi:10.20944/preprints202009.0507.v1

given weights subjectively by the author. The purpose of this multi-criteria analysis was to choose the best material pair variant to achieve the optimum seal performance, ring geometry and system temperature. **Error! Reference source not found.** summarizes the criteria selected for the analysis.

Table 1. Criteria for analysis.

			Materials					
Criteria	**Unit**	**Weight ω**	**Alumina-SiC**	**RiC-SiC**	**SiC-SiC**	**Alumina-WC**	**RiC-WC**	**WC-WC**
Performance								
Volumetric flow rate	(m^3/h)	$0.25(-)$	3.08E-8	2.64E-8	2.15E-8	5.20E-8	4.48E-8	3.91E-8
Power loss	$(N\,m/s)$	$0.15(-)$	1480	1550	1650	1160	1210	1250
Opening force	(N)	$0.2(+)$	436	428	415	455	447	439
Geometry								
Minimum radial clearance	(m)	$0.2(-)$	1.58E-6	1.52E-6	1.43E-6	1.72E-6	1.66E-6	1.6E-6
Temperature								
Difference in fluid temperature	(^{o}C)	$0.2(-)$	22.2	23.9	22.5	32.3	33.7	28.5

The criteria used in the multi-criteria analysis can be expressed by means of measurable or unmeasurable parameters. All the criteria are given dimensionless numerical values to assess and compare the selected variants. The process of replacing dimensional values with dimensionless values is called normalization. Normalization may involve maximizing the variables (stimulants $(+)$) or minimizing them (destimulants $(-)$). Signs $(+)$ and $(-)$ are given in **Error! Reference source not found.** next to the values of the weights.

The variants are rated on the basis of the synthetic estimates S_i, which are calculated using the summation index, taking into consideration the weights of the particular criteria determined according to the formula:

$$S_i = \sum_{j=1}^{m} x_{ij}^{*}\,\omega_j \tag{39}$$

The final estimate of the analyzed variants is calculated by reducing the sum of S_i to a unity according to the following formula:

$$S_i^{*} = S_i / \sum_{i=1}^{n} S_i \tag{40}$$

The most favorable variant is that with the highest S_i^{*}.

Table 2. Method for the criteria normalization.

Normalization Method	**Maximization (stimulants)**	**Minimization (destimulants)**
Van Delft and Nijkamp approach	$x_{ij}^{*} = \dfrac{x_{ij}}{\sqrt{\sum_{i=1}^{n} x_{ij}^{2}}}$	$x_{ij}^{*} = 1 - \dfrac{x_{ij}}{\sqrt{\sum_{i=1}^{n} x_{ij}^{2}}}$

Preprints (www.preprints.org) | NOT PEER-REVIEWED | Posted: 22 September 2020 doi:10.20944/preprints202009.0507.v1

Error! Reference source not found. explains the method for criteria normalization with the notations being as follows: x_{ij}^{*} – normalized value of the i-th variant satisfying the j-th criterion and x_{ij} – value of the i-th variant satisfying the j-th criterion.

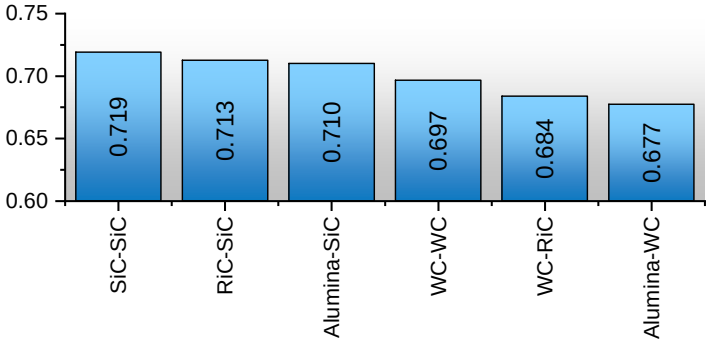

Figure 8. Results of the multi-criteria analysis.

The calculation results obtained using the Van Delft and Nijkamp normalization method indicate that, for the predetermined heat transfer conditions and seal performance parameters, the volumetric flow rate is the lowest when both rings made of silicon carbide (**Error! Reference source not found.**).

The multi-criteria analysis is suitable for facilitating the decision-making process in situations when there are many variants to consider and/or the results do not give a clear best choice.

Conclusion

Sealing systems, which are crucial elements of many industrial machines, need to be designed in such a way that they conform to stringent safety standards if hazardous substances are used as process fluids.

Non-contacting face seals have numerous applications mainly because they meet divergent demands concerning both efficient performance and environmental safety. The major requirement to be met by seals is to maintain leak-tightness, irrespective of changes in the internal factors. Meeting this condition, however, is extremely difficult and one of the reasons for this may be changes in the geometry of the radial clearance caused by thermal deformations. Such deformations are likely to result in a disturbance to the equilibrium of forces, i.e., an increase in the opening force, which contributes to a higher leakage rate.

There is a direct relationship between the radial clearance geometry, the equilibrium of forces acting on the sealing rings, the leakage rate and the power loss. A change in any of these parameters may result in the disturbances to the performance of the whole sealing system, and consequently a failure of the machine in which the seal is installed.

Effectiveness of a seal depends on a number of factors. First of all, it is essential to select the right type of seal for a given application. Then, at the design stage, it is necessary to specify the desired temperature of the fluid film and the rings. It is also vital to predict the thermal deformations of the rings in order to prevent excessive wear of their surfaces as well as uncontrolled fluid leakage or power loss.

Funding: This research received no external funding

Conflicts of Interest: Declare conflicts of interest or state “The authors declare no conflict of interest.” Authors must identify and declare any personal circumstances or interest that may be perceived as inappropriately influencing the representation or interpretation of reported research results. Any role of the funders in the design of the study; in the collection, analyses or interpretation of data; in the writing of the manuscript, or in the decision to publish the results must be declared in this section. If there is no role, please state “The funders had no role in the design of the study; in the collection, analyses, or interpretation of data; in the writing of the manuscript, or in the decision to publish the results”.

References

1. Pascovici, M.D.; Etsion, I. A thermohydrodynamic analysis of a mechanical face seal. *ASME Journal of Tribology* **1992**, *1992*, 639–645.
2. Tournerie, B.; Danos, J.C.; Fre^ne, J. Three-Dimensional Modeling of THD Lubrication in Face Seals. *Journal of Tribology* **2001**, *123*, 196, doi:10.1115/1.1327584.
3. Brunetière, N.; Tournerie, B.; Frêne, J. TEHD Lubrication of Mechanical Face Seals in Stable Tracking Mode: Part 2—Parametric Study. *Journal of Tribology* **2003**, *125*, 617, doi:10.1115/1.1510886.
4. Brunetière, N.; Tournerie, B.; Frêne, J. TEHD Lubrication of Mechanical Face Seals in Stable Tracking Mode: Part 1—Numerical Model and Experiments. *Journal of Tribology* **2003**, *125*, 608, doi:10.1115/1.1510885.
5. Blasiak, S.; Kundera, C. A Numerical Analysis of the Grooved Surface Effects on the Thermal Behavior of a Non-Contacting Face Seal. *Procedia Engineering* **2012**, *39*, 315–326.
6. Blasiak, S.; Kundera, C.; Bochnia, J. A Numerical Analysis of the Temperature Distributions in Face Sealing Rings. *Procedia Engineering* **2012**, *39*, 366–378.
7. Li, C.-H. Thermal Deformation in a Mechanical Face Seal. *A S L E Transactions* **1976**, *19*, 146–152, doi:10.1080/05698197608982788.
8. Banerjee, B.N. The influence of thermoelastic deformations on the operation of face seals. *Wear* **1980**, *59*, 89–110, doi:10.1016/0043-1648(80)90272-0.
9. Etsion, I.; Pascovici, M.D. A Thermohydrodynamic Analysis of a Misaligned Mechanical Face Seal. *Tribology Transactions* **1993**, *36*, 589–596, doi:10.1080/10402009308983199.
10. Gu, B.; Zhou, J.; Chen, Y.; Sun, J. Frictional heat transfer regularity of the fluid film in mechanical seals. *Science in China Series E: Technological Sciences* **2008**, *51*, 611–623, doi:10.1007/s11431-008-0045-5.
11. Blasiak, S. Time-fractional heat transfer equations in modeling of the non-contacting face seals. *International Journal of Heat and Mass Transfer* **2016**, *100*, 79–88, doi:10.1016/j.ijheatmasstransfer.2016.04.040.
12. Blasiak, S. Heat transfer model for the wavy-tilt-dam mechanical seals using Green's Function Method. In *ENGINEERING MECHANICS 2017*; ACAD SCI CZECH REPUBLIC, INST THERMOMECHANICS: DOLEJSKOVA 5, PRAGUE 8, 182 00, CZECH REPUBLIC, 2017; pp 158–161, ISBN 978-80-214-5497-2.
13. J. Zhou; B. Gu; Y. Chen. An Improved Design of Spiral Groove Mechanical Seal. *Chinese Journal of Chemical Engineering* **2007**, *15*, 499–506.
14. Noda, N.; Hetnarski, R.B.; Tanigawa, Y. *Thermal stresses*, 2nd ed.; Taylor & Francis: New York, 2003, ISBN 9781560329718.
15. Strąk, K.; Piasecka, M.; Maciejewska, B. Spatial orientation as a factor in flow boiling heat transfer of cooling liquids in enhanced surface minichannels. *International Journal of Heat and Mass Transfer* **2018**, *117*, 375–387, doi:10.1016/j.ijheatmasstransfer.2017.10.019.
16. Du, Q.; Gao, K.; Di Zhang; Xie, Y. Effects of grooved ring rotation and working fluid on the performance of dry gas seal. *International Journal of Heat and Mass Transfer* **2018**, *126*, 1323–1332, doi:10.1016/j.ijheatmasstransfer.2018.05.055.
17. Kukla, S.; Siedlecka, U. Fractional heat conduction in a sphere under mathematical and physical Robin conditions. *jtam* **2018**, 339, doi:10.15632/jtam-pl.56.2.339.
18. Maciejewska, Beata and Piasecka, Magdalena. An application of the non-continuous Trefftz method to the determination of heat transfer coefficient for flow boiling in a minichannel. *Heat and Mass Transfer* **2017**, *53*, 1211–1224, doi:10.1007/s00231-016-1895-1.
19. Ruan, B. Numerical Modeling of Dynamic Sealing Behaviors of Spiral Groove Gas Face Seals. *J. Tribol* **2002**, *124*, 186, doi:10.1115/1.1398291.